MODELING THE LEFT HEART: FINITE ELEMENT ANALYSIS AND FLUID STRUCTURE INTERACTION SIMULATION ON MITRAL REGURGITATION PATIENT IMAGES

A Thesis
Presented to
The Academic Faculty

by

Hannah Danielle Geil

In Partial Fulfillment
of the Requirements for the Degree
Bachelor of Science in the
School of Biomedical Engineering

Georgia Institute of Technology
August 2019

COPYRIGHT 2019 BY HANNAH GEIL

MODELING THE LEFT HEART: FINITE ELEMENT ANALYSIS AND FLUID STRUCTURE INTERACTION SIMULATION ON MITRAL REGURGITATION PATIENT IMAGES

Approved by:

Dr. Wei Sun, Advisor
School of Biomedical Engineering
Georgia Institute of Technology

Dr. Tongran Qin
School of Biomedical Engineering
Georgia Institute of Technology

Dr. James Stubbs
School of Biomedical Engineering
Georgia Institute of Technology

ACKNOWLEDGEMENTS

I wish to thank my research mentor, Dr. Tongran Qin, as well as the head of the Tissue Mechanics Lab, Dr. Wei Sun. I would also like to that Andres Caballero for guidance and help with the research. Finally, I would like to thank my parents, Mark and Amy Geil for continuous support in every aspect of my life.

TABLE OF CONTENTS

LIST OF FIGURES AND TABLES

ABSTRACT

Mitral regurgitation affects over two million people in the US and can lead to heart failure, so research is needed to predict, diagnose, and treat this valvular disease. Thus, cardiac modeling *in vitro* includes mathematical, automated, and image-based models. Mathematical modeling requires assumptions that make it less accurate, and it takes too long to conduct to be clinically relevant. Automated modeling is faster but generally untrusted in the field. Image-based models are often patient specific and accurate but are rarely combined with computational models. Due to a need for an accurate and comprehensive model, this study used image-based modeling techniques and computational simulations of blood flow. Patient-specific images were used to create a three-dimensional model of the left heart. After segmentation, meshing, and defining boundary conditions, the model was run though a finite element analysis and a fluid structure interaction simulation. Nodes were then quantified to understand how the heart responded to simulation. Results showed that as pressure increased, stress and strain increased, and regurgitation area decreased. The results of this study have direct clinical applications; physicians can use the models as a guide when making decisions regarding diagnoses or surgical treatment.

CHAPTER 1

INTRODUCTION

The mitral valve (MV) is one of the most complex valves in the heart, consisting of two leaflets, a mitral annulus, and cordae tendineae. Its important role in regulating blood flow between the left atrium and ventricle means that dysfunction of the MV could lead to heart failure and death (1). The most commonly seen MV dysfunction is mitral regurgitation (MR), affecting over 2 million people in the United States. MR occurs when blood leaks from the left ventricle (LV) to the left atrium (LA) when the MV should be closed (2). To better diagnose and treat mitral regurgitation and other valvular disorders, researchers create models of the MV (3). Various components of the heart (walls, valves, atria, ventricles) have been modeled with techniques including simple math models, image-based models, and automated modeling (4-6).

Mathematical Modeling

Mathematical modeling has progressed and advanced in recent years. For example, a strain energy function (SEF) was developed to characterize the nonlinear hyperelastic properties of a vessel near the mitral valve to better understand mitral regurgitation (7). In another study, a model based on Navier-Stokes equations combined with a spring-mass model serving as a structural solver provided a way to characterize stenosis (8). A newly created electro-mechano-fluidic model has improved on conventional computational dynamics models by incorporating finite element modeling (9). In general, math models require generous simplifications and take too much time to conduct, limiting their usefulness for surgical predictions (8).

Automated Modeling

To create models that shorten the time required to provide predictions before surgeries, researchers have explored automated modeling with the use of artificial

intelligence. Pouch et al. compared the data from their automated model to data from a model manually created by an expert. They found that the automatic segmentation was similar to the manual, but no statistical analysis was conducted (6). Jeganathan et al. performed an experiment to determine if different users of a machine learning automated valvular analysis program would have different results. After analyzing their data, they found that the examiner did not statistically impact any of the six parameters they tested, indicating that it is possible to use automated computer programs to analyze the mitral valve. These researchers noted, though, that a general skepticism towards automated modeling make it less used than manual modeling (5).

Image-Based Modeling

In addition to mathematical models and automated models, image-based models are used to view and understand valvular dynamics (1; 4). Image-based models range from echocardiography to magnetic resonance imaging, and they can be used in both two-dimension and three-dimension views. In many image based models, only the valve being studied is modeled, not the surrounding area (10). Some incorporate fluid structure interactions, but many are not combined with computational models (4). Few studies exist that combine computational (image-based modeling with simulations) and experimental research (10). When considering both the diagnosis and treatment of cardiac diseases, a patient-specific, multifaceted approach is most useful to create accurate predictions about valvular function and dynamics. Ensuring that the tissue properties observed in the lab match those included in the computational modeling gives the research validation (11).

Thus, this study expanded on the existing modeling techniques for the left heart by providing an accurate and comprehensive approach. Image-based models that are patient specific will be used in computational models and run through simulations to mimic blood flow. This computational research will occur in conjunction with experimental tissue research to provide a comprehensive view of the left heart.

CHAPTER 2

MATERIALS AND METHODS

Methods included segmentation and mesh generation to create a model including the left ventricular walls, aorta, atrial valve (AV), mitral valve (MV), and calcification. Finite element simulation was conducted to analyze stress and strain for the effect of calcification and loading conditions.

Patient Information

De-identified patient specific cardiac multi-slice computed tomography (MSCT) scans were obtained from Hartford Hospital in Hartford, CT in addition to Institutional Review Board approval to review these images. Patients were scanned to diagnose MR, and data from the scans included all cardiac cycle phases.

Approximately 2000 image slices from each patient were reconstructed into 10 phases of the cardiac cycle and separated into axial, coronal, and sagittal views. The full volume CT images were acquired from a GE LightSpeed 64-channel volume CT scanner with an in-plane resolution of 0.82×0.82 mm and a slice thickness of 0.625 mm.

Segmentation

For both the valves and the cardiac wall, first a rough segmentation was completed, then a smooth segmentation. First, mid-diastole and mid-systole phases were identified. For the valves, calcification, and aorta, the images were imported into Avizo software (Thermo Fisher Scientific, MA). Labels were created, the magic wand tool was used for rough segmentation, and the paint tool was used to make the segmentations more accurate and smoother. Segmentation, shown in Figure 1, was repeated for the leaflets and calcification.

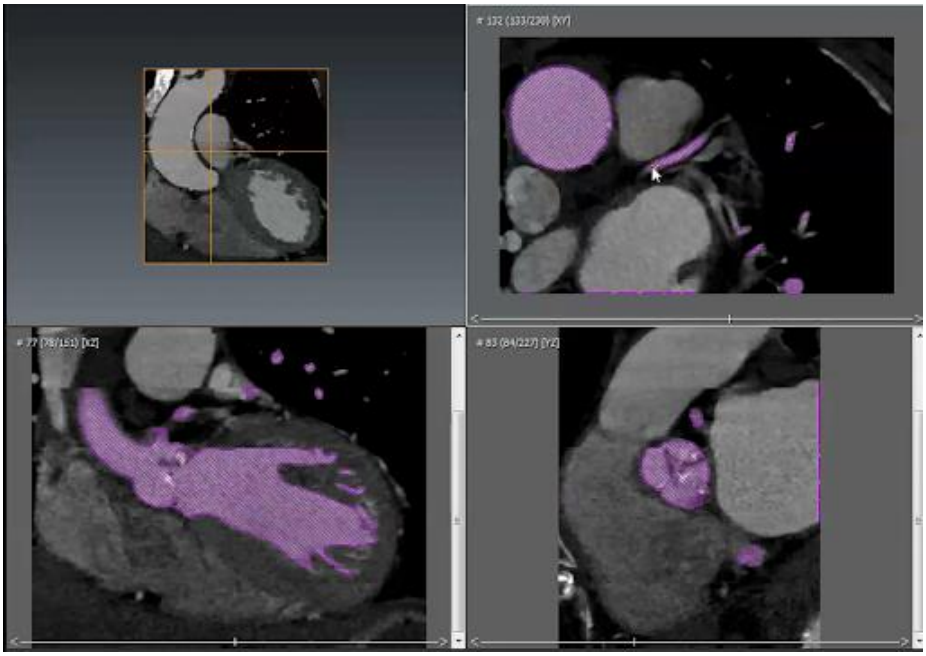

Figure 1: Four views of aortic valve segmentation in Avizo

For the heart wall, images were imported into 3D Slicer and roughly segmented using the threshold tool. Rough segmentation was repeated for each phase with the same threshold parameters. Then, each phase was modified using segment editor, paint, and smoothing functions until a smooth mesh was made, as shown in Figure 2.

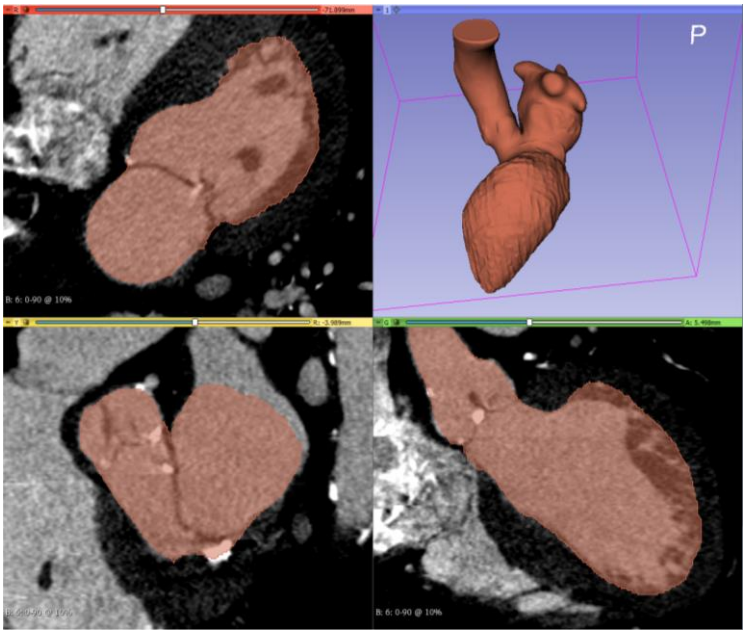

Figure 2: Four views of left ventricular wall meshing in 3D Slicer

Mesh Generation

Next, the computational mesh of left ventricular walls, aorta, AV, MV, and calcification was generated in Hypermesh (Altair Engineering, Inc., MI). Smooth segmentations were imported, and nodes were specified. After lines were generated to connect the nodes, a spline surface was created. Then, a mesh was generated using automesh. The element types can be found in Table 1.

Component	Element type	Element classification	Element description	Number of elements
LH	S4R	2-D shell element	3-node triangular	24005
MV	C3D8R	3-D solid element	8-node linear brick	17979
	C3D8I	3-D solid element	8-node linear brick, incompatible modes	
	C3D6	3-D solid element	6-node linear triangular prism	
MV chordae tendineae	T3D2	3-D stress/displacement truss elements	2-node linear displacement	706
MV Calcification	C3D4	3-D solid element	4-node linear tetrahedron	436266
	C3D8R	3-D solid element	8-node linear brick	

Table 1: Element type and number for different components of the model

After the mesh was generated, the existing mesh was matched to the surface it connected to using hypermorph. Finally, sets were defined with distinguishing colors, shown in Figure 3.

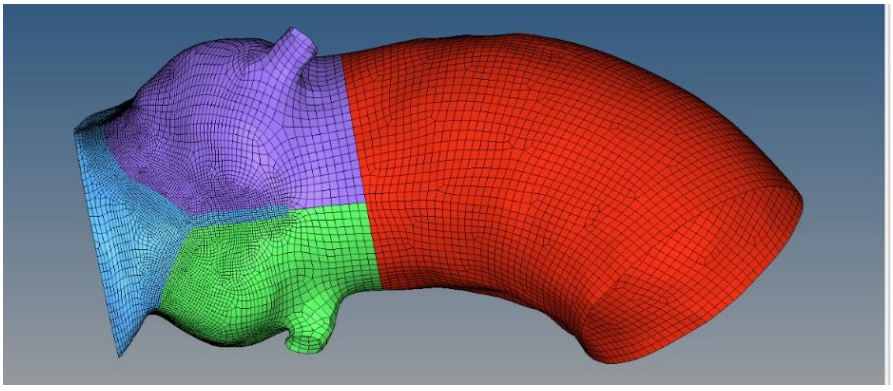

Figure 3: Meshed aortic valve in Hypermesh, split into four sets

Finite Element Analysis

The last step was to set up and perform the simulation. The meshed surfaces were imported into Abaqus/Explicit (SIMULIA, Providence, RI) so that sets, surfaces, sections, orientations, material properties, and datum cys could be defined. For the material properties, the mechanical behavior of the MV leaflet tissues was based on an anisotropic hyperelastic material model, which was first proposed by Holzapfel et al (12; 13).

Once the simulation was set up, the simulation was performed in two steps. First, boundary conditions were applied to simulate pretension. For the finite element analysis, the motion of diastole and systole were simulated, and nodal positions were approximated at each state. Second, pressure was applied in wave form as shown in Figure 4. The peak pressures for the low, normal, and high pressure cases were 100, 120, and 140 mmHg, respectively. The pressure applied simulated valve closure from diastole to systole, thus completing the simulation of the cardiac cycle.

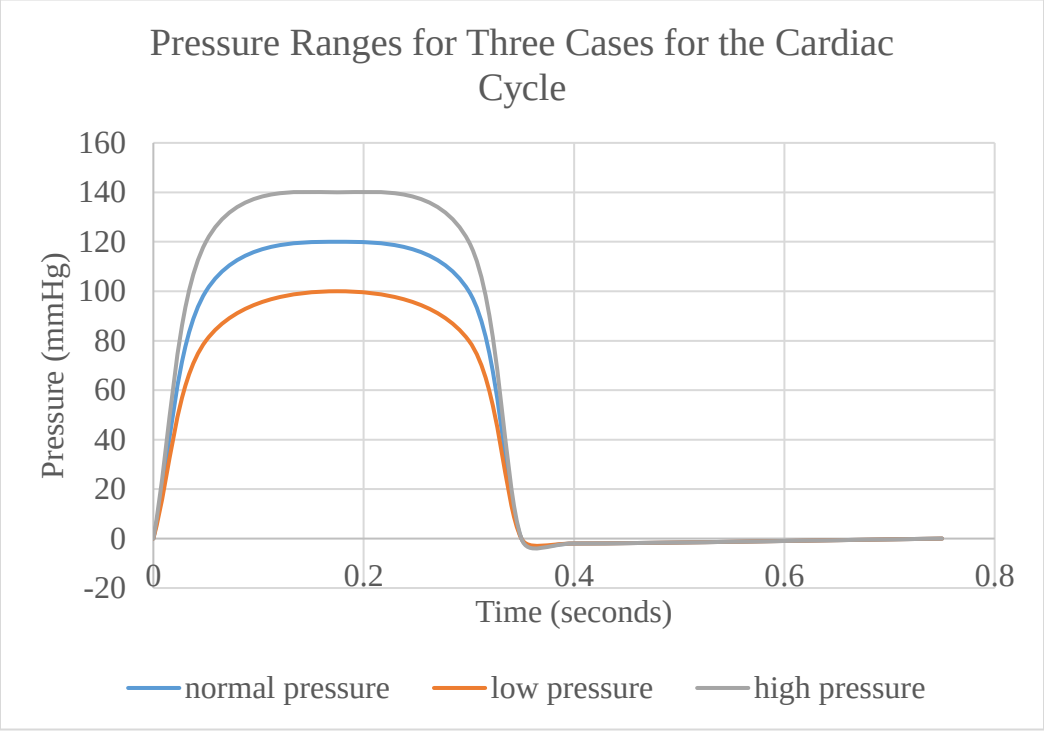

Figure 4: Pressure over time for three cases

Chordal Length Adjustments

Chordal length was iteratively adjusted to closely match the MSCT images, making the model more accurate to the heart under systolic pressure. FE model accuracy was assessed using the deformed FE models and image geometry's point-to-mesh distance error. Following previously published methods for the MV, the curvature of the chords was increased and decreased while the insertion and origin points were stationary to adjust the chordal lengths (14).

CHAPTER 3

RESULTS

Results came from analyzing the computational model at end-systole for a high pressure, low pressure, and normal pressure case. The three pressure distributions can be seen in Figure 4, displaying pressure over time for the entire cardiac cycle, which lasted 0.75 seconds. End-systole was at 0.3 seconds. Figure 5 shows an atrial view of the MV deformed FE geometry at normal pressure overlaid on the end systole MSCT images. The superimposition shows a good overall agreement between the computational model and the ground truth MSCT model.

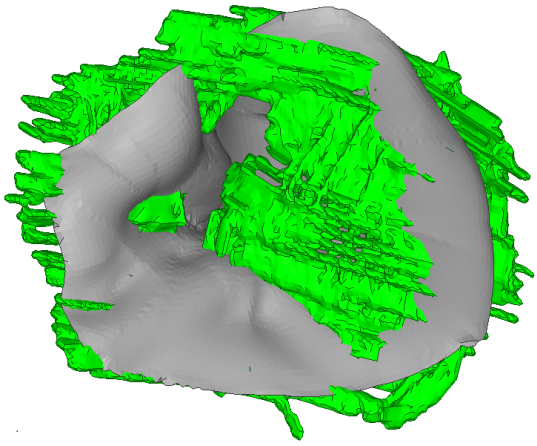

Figure 5: FE model (grey) overlapped with MSCT image model (green) at end systole

The maximum principle stress distribution of mitral leaflets at three different levels of pressure are shown in Figure 6. All three are shown at end-systole. The red regions, shown primarily on the anterior mitral leaflet (AML), indicate areas of higher stress. The posterior mitral leaflet (PML) generally had blue, or low stress regions.

Normal Pressure	High Pressure	Low Pressure

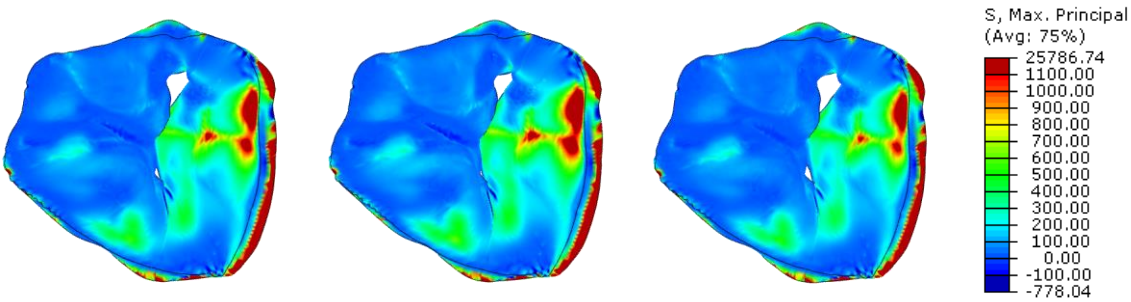

Figure 6: Contour map of maximum principal stress distribution on the mitral leaflets

The average, maximum, and minimum principal stresses were calculated for each pressure case, excluding the top 1% of the data to account for outliers. The averages for tensile stress for the AML and the PML for each case are shown in Figure 7. The largest average tensile stress, 210.27 kPa, was seen in the high-pressure case near the attachment line of the AML.

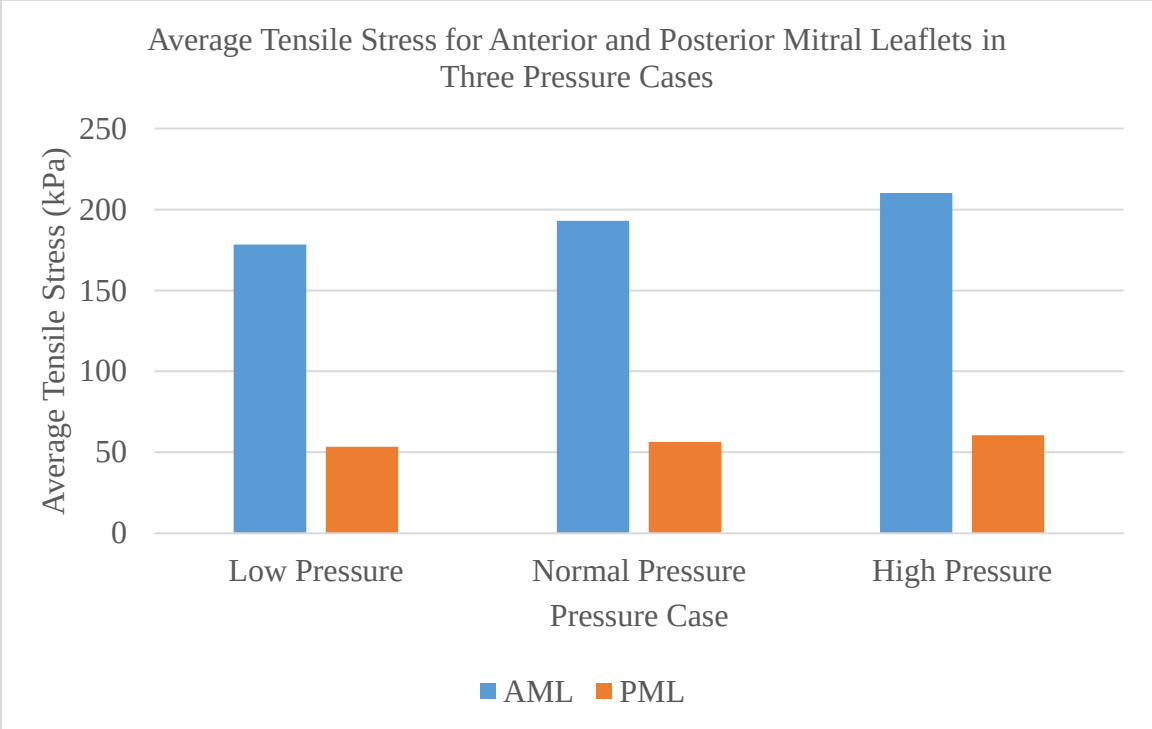

Figure 7: Average tensile stress for PML and AML in each pressure case

The averages for the compressive stress are shown in Figure 8. Larger negative values of compressive stress were seen in the PML when compared to the AML. Thus, the PML had larger compressive stress values than the AML.

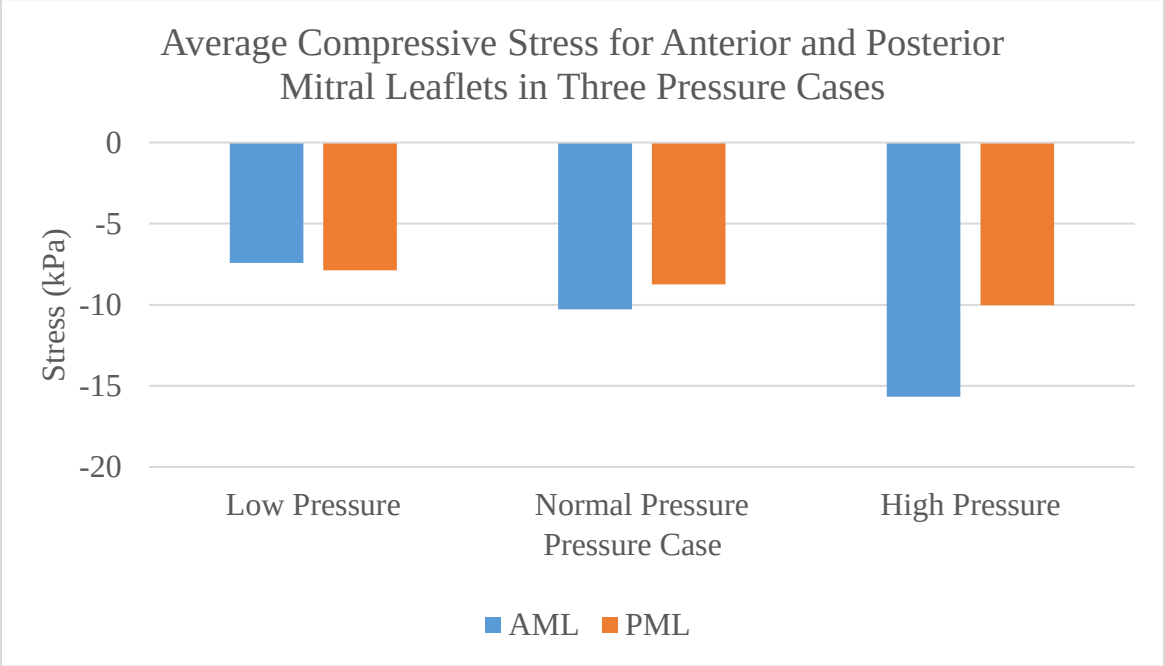

Figure 8: Average compressive stress for AML and PML in each pressure case

Figure 9 shows the strain distributions at end-systole of mitral leaflets at three different levels of pressure. The limits ranged from 0 to 0.4 for the maximum principal strain contour, and red regions indicated larger strain values. More red regions, indicating larger strain values, were seen in the AML than in the PML.

Normal Pressure	High Pressure	Low Pressure

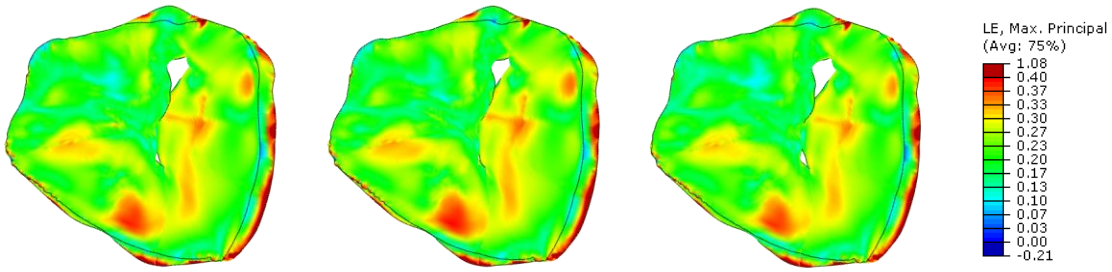

Figure 9: Contour map of maximum principal strain of mitral leaflets

The average maximum principal strain was computed for the AML and PML for each pressure case. Overall, average AML maximum principle strain for low pressure, normal pressure, and high pressure were 0.248, 0.251, and 0.254 respectively, shown in Figure 10. The average strain values for the AML were higher than those of the PML, which had values for low pressure, normal pressure, and high pressure of 0.217, 0.219, and 0.221 respectively.

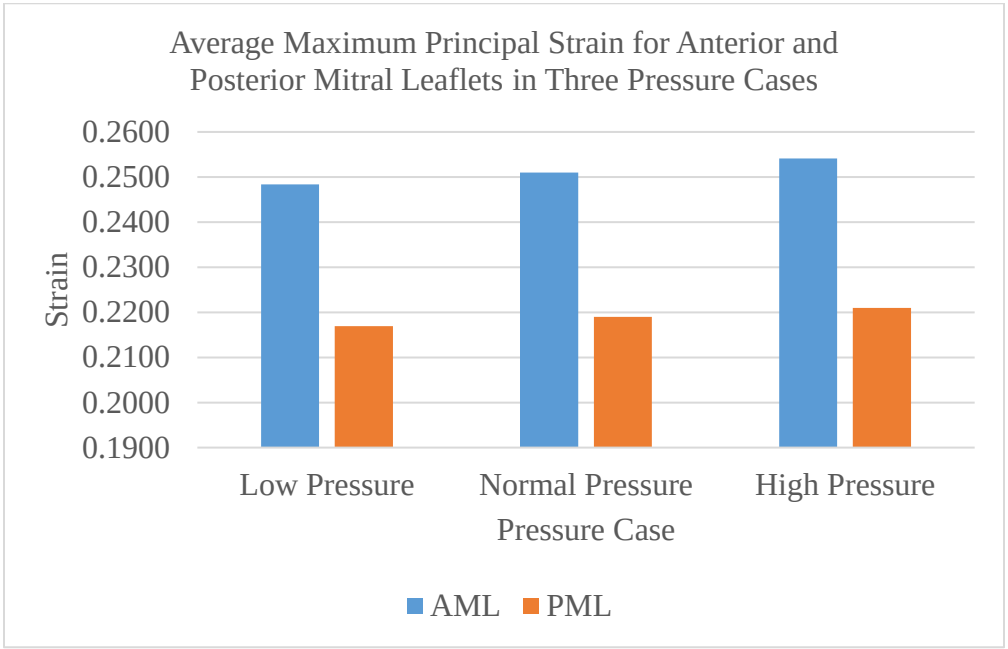

Figure 10: Average maximum principal strain for each pressure case

CHAPTER 4

DISCUSSION

Computational models combined with image-based models can quantify mitral regurgitation biomechanics and inform treatment decisions. This study showed a model of the left heart that underwent three different pressure cases during simulation. The results showed that as pressure increased, values of stress and strain increased, as expected.

The average principal tensile stress for all three pressure cases were larger for the AML than for the PML, which could be due to the movement of the mitral annulus during the cardiac cycle. This movement caused the MV to be corrugated, being compressed on the PML side and stretched on the AML side. This also could explain why the largest maximum principal stress values were seen on the attachment line of the AML, and why the larger compressive stress values were seen in the PML.

Other causes for stress and strain on the MV include the calcification attachment and the tethering forces caused by chordae tendineae. These forces created local maximum values of stress and strain, but the overall trends observed were more likely caused by the corrugation of the valve.

The model created came from images of a mitral regurgitation patient, which is evident by the unclosed valves observed at end systole, shown in Figure 6 and Figure 9. These figures also show that as pressure increased, the area of regurgitation decreased. Relating these pressure findings to blood pressure in patients could have clinical implications for physicians making MR treatment decisions.

Limitations

Despite using patient-specific images, physiological boundary conditions, and representative material properties, some assumptions were required for this model. Because the MSCT images had limited resolution, the detailed choral origins and

insertion locations had to be estimated. However, with these estimations, the model could simulate full closer at systole, suggesting the assumptions were rational. Additionally, experimental measurements, not imaging data, were used to estimate leaflet thickness. This did not account for individual variation of leaflet thickness. In addition to thickness, the leaflet material properties were assumed based on a cadaver study, rather than the patients' material properties (15). Finally, the study time frame was not rapid enough to be used in a clinical setting. The manual segmentation and simulation take approximately five hours to complete for each model. Future research would need automated model generation to be relevant for clinical use.

CHAPTER 5

CONCLUSION

This study included a left heart model with patient-specific geometries reconstructed from MSCT images. The model represented a good match to the MSCT data at end systole after adjusting chordal lengths iteratively. Insight into mitral regurgitation biomechanics was gained from the model's quantitative measurements of leaflet stress and strain and from the relationship found between pressure and regurgitation area. Future studies could use this model to simulate treatments, which could give insight into device design and cardiac surgeon decision making to understand how best to treat mitral regurgitation.

APPENDIX A

SIMULATION RESULTS AT EACH CARDIAC CYCLE STEP

Frame 0	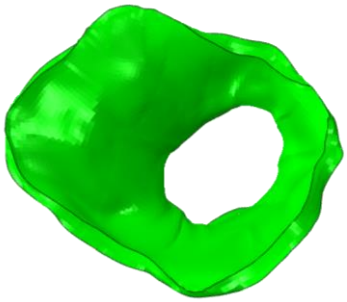	Frame 45	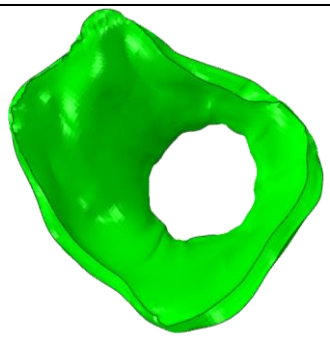
Frame 15		Frame 60	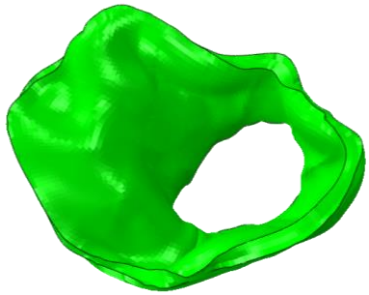
Frame 30	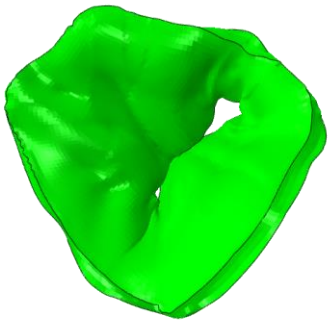	Frame 75	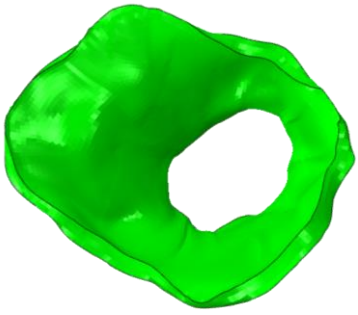

REFERENCES

1. Gao H, Qi N, Feng L, Ma X, Danton M, et al. 2017. Modelling mitral valvular dynamics–current trend and future directions. *International Journal for Numerical Methods in Biomedical Engineering* 33:e2858
2. Piérard LA, Carabello BA. 2010. Ischaemic mitral regurgitation: pathophysiology, outcomes and the conundrum of treatment. *European Heart Journal* 31:2996-3005
3. de Marchena E, Badiye A, Robalino G, Junttila J, Atapattu S, et al. 2011. Respective prevalence of the different carpentier classes of mitral regurgitation: a stepping stone for future therapeutic research and development. *Journal of cardiac surgery* 26:385-92
4. Sun W, Martin C, Pham T. 2014. Computational Modeling of Cardiac Valve Function and Intervention. *Annual Review of Biomedical Engineering* 16:53-76
5. Jeganathan J, Knio Z, Amador Y, Hai T, Khamooshian A, et al. 2017. Artificial intelligence in mitral valve analysis. *Annals of cardiac anaesthesia* 20:129-34
6. Pouch AM, Wang H, Takabe M, Jackson BM, Gorman JH, 3rd, et al. 2014. Fully automatic segmentation of the mitral leaflets in 3D transesophageal echocardiographic images using multi-atlas joint label fusion and deformable medial modeling. *Medical image analysis* 18:118-29
7. Pham T, Sun W. 2010. Characterization of the mechanical properties of the coronary sinus for percutaneous transvenous mitral annuloplasty. *Acta Biomaterialia* 6:4336-44
8. Meschini V, Viola F, Verzicco R. 2019. Modeling mitral valve stenosis: A parametric study on the stenosis severity level. *Journal of Biomechanics* 84:218-26
9. Karabelas E, Gsell MAF, Augustin CM, Marx L, Neic A, et al. 2018. Towards a Computational Framework for Modeling the Impact of Aortic Coarctations Upon Left Ventricular Load. *Frontiers in Physiology* 9
10. Ayoub S, Lee C-H, Driesbaugh KH, Anselmo W, Hughes CT, et al. 2017. Regulation of valve interstitial cell homeostasis by mechanical deformation: implications for heart valve disease and surgical repair. *Journal of the Royal Society, Interface* 14:20170580
11. Stähli BE, Reinthaler M, Leistner DM, Landmesser U, Lauten A. 2018. Transcatheter Aortic Valve Replacement and Concomitant Mitral Regurgitation. *Frontiers in Cardiovascular Medicine* 5:1-9
12. Gasser TC, Ogden RW, Holzapfel GA. 2006. Hyperelastic modelling of arterial layers with distributed collagen fibre orientations. *J R Soc Interface* 3:15-35
13. Holzapfel G, Gasser T, Ogden RW. 2000. *A New Constitutive Framework for Arterial Wall Mechanics and a Comparative Study of Material Models*.
14. Pham T, Kong F, Martin C, Wang Q, Primiano C, et al. 2017. Finite Element Analysis of Patient-Specific Mitral Valve with Mitral Regurgitation. *Cardiovasc Eng Technol* 8:3-16
15. Lim KO. 1980. Mechanical properties and ultrastructure of normal human tricuspid valve chordae tendineae. *The Japanese journal of physiology* 30:455-64